IN-24

309

P-33
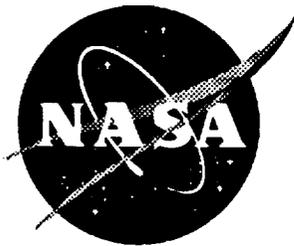
NASA Contractor Report 191590

Fatigue Resistance of Unnotched and Post-Impact [± 30°/0°] 3-D Braided Composites

M. A. Portanova
Lockheed Engineering & Sciences Company, Hampton, Virginia

National Aeronautics and
Space Administration
Langley Research Center
Hampton, Virginia 23681-0001

Abstract

The fatigue resistance of a multiaxial braided (3-D) graphite/epoxy composite in both unnotched and post impacted conditions has been evaluated. The material tested is a [±30°/0°] multiaxial braid constructed from AS4 / 12K tow graphite fibers and British Petroleum E905L epoxy resin. These materials were braided as dry preforms and the epoxy was added using a resin transfer moulding process (RTM). The unnotched and post-impact specimens were tested in compression-compression fatigue at 10 Hz with a stress ratio of R=10. The unnotched tension-tension fatigue specimens were tested at 5 Hz with a stress ratio of R=0.1. Damage initiation and growth was documented through the application of radiography and ultrasonic through transmission (C-scans). Visible inspection of surface and edge damage was also noted to describe the initiation and progression of damage in these materials. The mechanisms leading to damage initiation were established and failure modes were determined. Stiffness and strength degradation were measured as a function of applied cycles. These 3-D braided composite results were compared to strain levels currently used to design primary structure in commercial aircraft composite components made from prepreg tape and autoclave cured.

Key Words:

Introduction

The potential application of advanced composite materials in aircraft structures is currently being investigated throughout the aerospace industry. Graphite/epoxy composites have many advantages for use as aircraft structural materials but are prone to a wide range of defects and damage which may significantly reduce their residual strength [1,2]. Damage resulting from impacts are probably the most insidious because they can cause reductions in strength while being difficult to detect. Textile composites have been suggested as candidate materials because of their inherent tolerance to impact damage. This paper will address the fatigue resistance of a multiaxial braided (3-dimensional) graphite/epoxy in both unnotched and post impacted forms. These materials were braided as dry preforms and the epoxy was added using a resin transfer moulding (RTM) process. The unnotched specimens were tested in both tension and compression fatigue. The post-impact specimens, which were impacted at three different impact energies, were cycled only in compression. Damage initiation and growth was documented through the application of radiography and ultrasonic through transmission (C-scans). Visible inspection of surface and edge damage was also noted so as to be able to accurately describe the initiation and progression of damage in these materials. The mechanisms leading to damage initiation were established and failure modes were determined. Stiffness and strength degradation were measured as a function of applied cycles. These 3-D braided RTM composite results were compared to strain levels currently used design primary structure in commercial aircraft composite componets made from prepreg tape and autoclave cured.

Description of Materials

The material tested is a [±30°/0°] multiaxial braid constructed from Hercules AS4/12K tow graphite fibers and E905L, a low viscosity epoxy resin manufactured by British Petroleum. The 3-D braided preforms were braided by Atlantic Research Company using an equal number of tows in each of the +30°, -30°, and 0° directions. The graphite tows were braided on a cylinder, in a single pass, at the desired thickness. The preform was then removed from the cylinder, slit down its length to form a flat panel and then lightly stitched along the cut edge to maintain the braid angle. This stitched edge was later trimmed off after panel fabrication. The dry fabric preform was resin transfer molded by Fiber Innovations, Inc. All plates were cured in the same mold resulting in uniform fiber volume fraction. Fiber volume fraction, from acid digestion, was 52.2%. Thickness varied between 5.92 mm (0.233 in.) and 6.15 mm (0.242 in.). The average was 6.10 mm (0.240 in.) for the compression (post-impact and unnotched) and 5.99 mm (0.235 in.) for the unnotched tension specimens.

Polished sections of the test material along the 0°, 90°, and both the ±30° braid angles were examined using a light microscope. It was obsedver that the 0° tows tend to be uniformly distributed through the thickness. Inspection of the ±30° braid angle showed the graphite tows traversing through the thickness, resulting in true through the thickness reinforcement. The 90° view shows that the 0° tows do not tend to nest, resulting in large, repeating resin rich regions, running along the length in the loading direction.

Photomicrographs of sections along the 0°, 90°, and both the ±30° braid angles are shown in Figure 1. The 0° tows tend to be uniformly distributed through the thickness. Inspection of the ±30° braid angle photomicrographs shows the graphite tows traversing through the thickness, resulting in true through the

3

thickness reinforcement. The 90° view shows that the 0° tows do not tend to nest, resulting in large, repeating resin rich regions, running along the length in the loading direction.
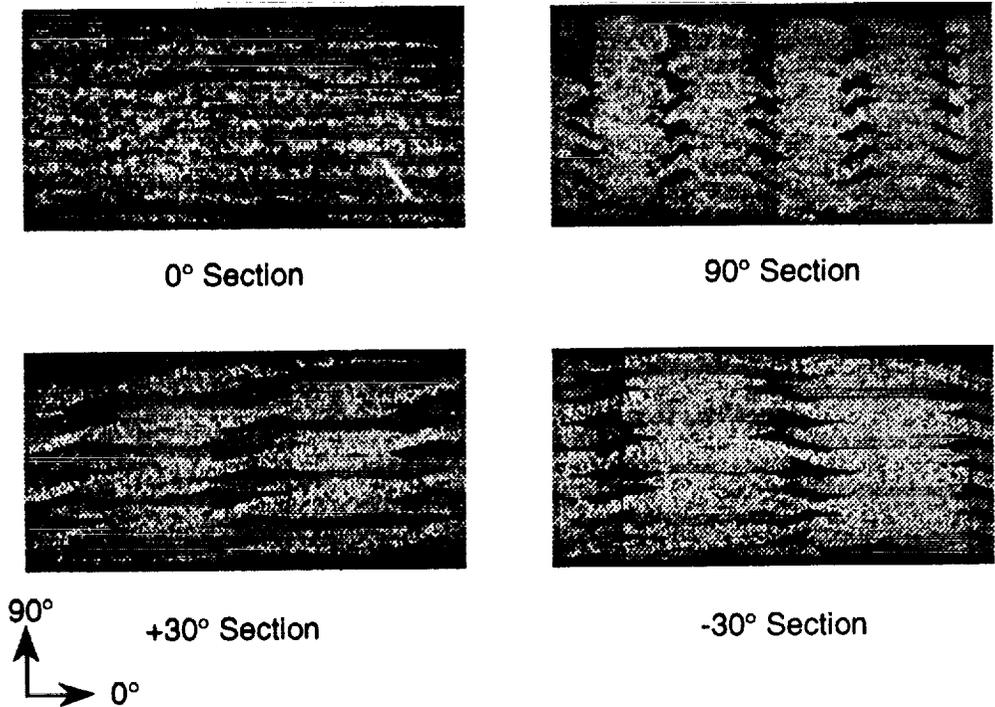

0° Section

90° Section

90°
↑
└→ 0°

+30° Section

-30° Section

Figure 1. Photomicrographs of 3-D Braided Architecture.

Test Specimens

Unnotched Fatigue Specimens

All specimens were machined from the panel with a diamond saw and all load bearing ends were ground smooth and parallel. A large radius was machined in the test section of the unnotched specimens to ensure that failure would be in the test section, not at the grip interface. The test section for both tension and compression fatigue specimens were reduced from an overall width of 38.1 mm (1.5 in.) to 25.4 mm (1.0 in.). An illustration of the tension and compression fatigue specimens is shown in Figure 2.
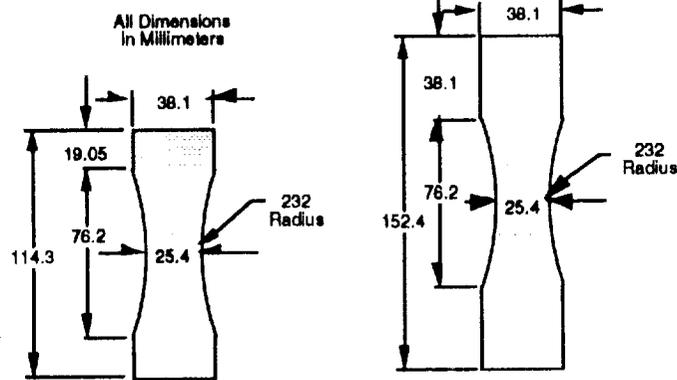
4

Figure 2. An Illustration of the Unnotched Fatigue Specimens.

The compression fatigue specimens were mostly end loaded so only a minimal amount of material was inserted in the hydraulic grips. Accordingly, steel plates, approximately 0.762 mm (0.03 inch) thinner than the compression specimen, were placed in the grips. These plates are shown in Figure 3. The specimen ends bore on the plates inside the hydraulic grips. Only a minimal amount of clamping pressure was used. Thus, the coupons were mostly end loaded without brooming deformation of the ends of the specimens. The gauge length was kept short at 76.2 mm (3.0 in.) to prevent buckling/instability.

The tension fatigue specimens were clamped tightly in the hydraulic grips using approximately 3.45 MPa (5000 psi) grip pressure in order to transfer the load into the specimen through friction. A large area of gripped surface was used (1450 mm^2, 2.25 in.^{2}) to prevent crushing. A sheet of abrasive material was placed between the grip surface and the specimen to reduce the likelihood of slipping. To insure that the gage length was constant, the tension specimens were also seated on top of steel plates similar to that illustrated in Figure 3.

5

Post-Impact Fatigue Specimens

Again all specimens were machined with a diamond saw and all load bearing ends were ground smooth and parallel. All of the post-impact specimens had a test section of 101.6 x 152.4 mm (4.0" x 6.0"). The compression fatigue specimens were end loaded in a specially designed NASA compression-after-impact test fixture which used knife edge supports to prevent buckling [4]. An illustration of this fixture and of the compression after impact specimen is shown in Figure 4.
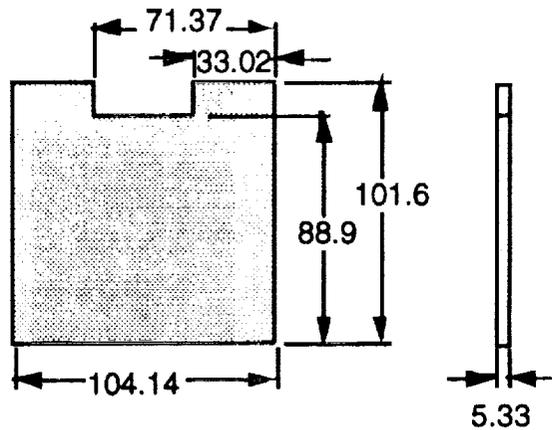
All dimensions in millimeters.

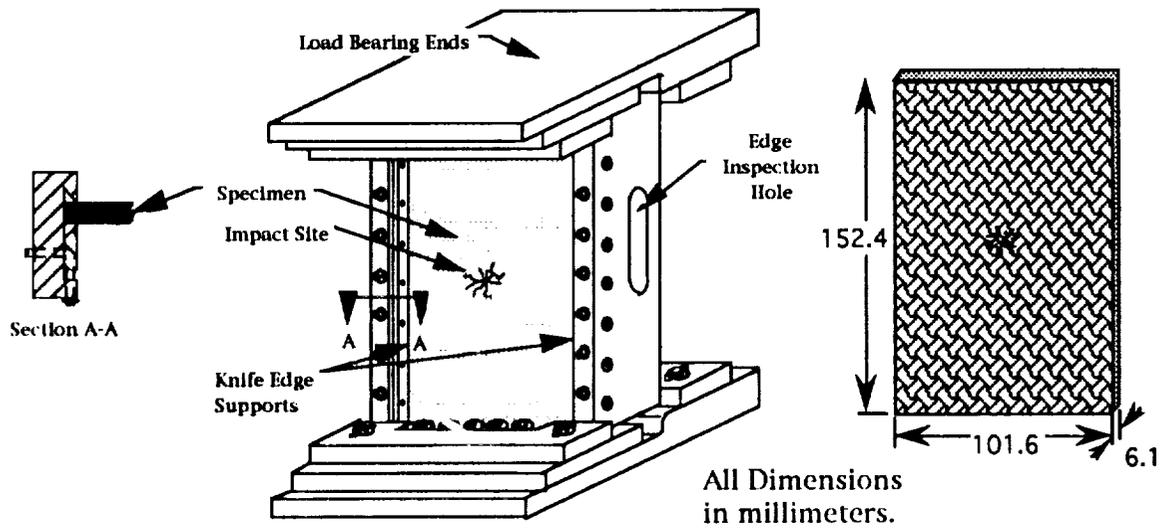Figure 3. Steel Shim Used to Endload Compression Specimens.

Figure 4. Post-Impact Compression Fatigue Test Fixture
and Specimen Geometry

Test Equipment and Procedures

Fatigue Testing

Fatigue tests were performed in a closed-loop servo-hydraulic testing machine in load-control mode.   Both compression-compression and tension-tension fatigue tests were conducted.   The unnotched compression-compression fatigue specimens were tested at 10 Hz with a stress ratio (minimum/maximum) of R=10. The unnotched tension-tension fatigue specimens and the post-impact compression-compression fatigue specimens were tested at 5 Hz with a stress ratio of R=0.1. All testing was conducted at room temperature ambient conditions.

A digital data storage oscilloscope was used to record load and stroke during testing. In addition, strain gages were mounted on the unimpacted test specimens. Before each fatigue test was run, a single monotonic excursion was made to maximum load. With the unimpacted fatigue specimens, the load was recorded

7

directly from the test stand load cell and strain was acquired either from a surface mounted strain gage or from the stroke output from the load frame. Only stroke output was recorded for the post-impact specimens because it better represented the global coupon deformation. A comparison was made between the stroke output and strain gage readings during a previous testing program of unnotched fatigue specimens [3]. Modulus measurements were found to agree quite well between the calculations using stroke and that from strain gages.

Strain gages provide a measure of the strain field, averaged under the gage. With textile composites, the strains on the surface will vary within the unit cell of the fiber architecture, where unit cell refers to the smallest repeating geometry of the textile architecture. The gage must be larger than a unit cell to provide an accurate homogenization of the strain. The unit cell of this 3-D braid was calculated to be 8.636 mm (0.340 inch) in the $0°$ direction, 4.98 mm (0.196 inch) in the $90°$ direction, and 0.706 mm (0.0278 inch) through the thickness. Therefore, 12.7 mm (0.5 inch) long by 4.57 mm (0.18 inch) wide strain gages were used for the majority of the fatigue test. Some fatigue specimens were tested with 25.4 mm (1.0 inch) long by 6.35 mm (0.25 inch) wide gages. For the monotonically loaded specimens, 6.35 mm (0.25 inch) long by 4.57 mm (0.18 inch) wide strain gages were used for the tension specimens and 3.175 mm (0.125 inch) long by 2.54 mm (0.10 inch) wide strain gages for the compression specimens. Some specimens were tested with $0°$ strain gages while others were tested with both $0°$ and $90°$ stacked gages to acquire Poisson's ratio. Poisson's ratio, for a few specimens, is reported in Table 2.

The slope of the load-versus-stroke plot was used to obtain the initial elastic modulus. A linear least squares fit (y=mx+b) was fit against the 1000 to 3000 $\mu\varepsilon$ data to determine modulus [3]. This process was repeated at various cycle counts throughout the

fatigue life and was used to monitor the change in stiffness of the specimens as a result of damage growth.

During testing of the unnotched fatigue specimens, the surface of the specimen was monitor visually to determine the initiation and progression of damage. With the post-impact specimens, dye penetrant enhanced radiography was used to monitor the increasing damage area at the same intervals as the stiffness loss data. Radiographs were taken and then converted into a digital format using a conventional desk top graphics scanner. These data files were then converted into binary data, threshold into two colors and then the ratio of dark to light pixels was calculated. This number could then be easily converted into an area measurement of the impact site. An example of the procedure is shown in Figure 5.
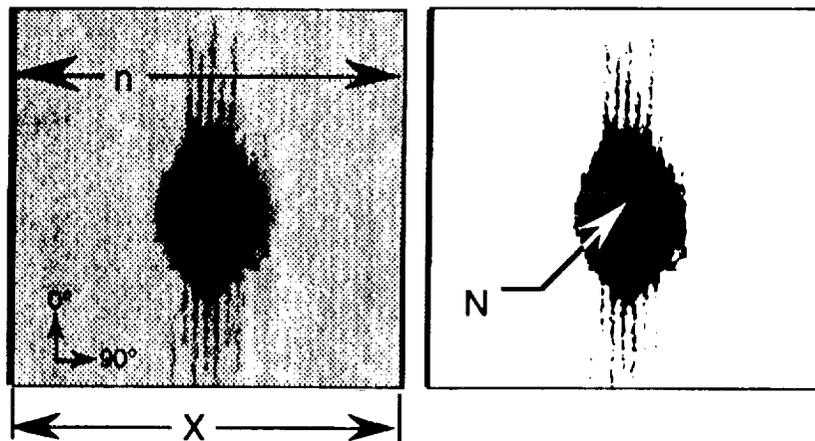
Where:
n = # of pixels across width
N = # of pixels in "Impact" area
Area = N $(X/n)^2$
and 4 in. is a known dimension

Figure 5. Area Measurements From Dye
Enhanced Radiography

Impacting Procedures

The test fixture used for the impact portion of this study contained a 127 mm (5 inch) by 76.2 mm (3 inch) opening with each corner radii of 12.70 mm (0.5 inch). A free falling mass of 5.31 kg (11.6 lbs) impacted the specimen. An illustration of a typical impactor set-up and test fixture is given in Figure 6. A methodology similar to that originally developed by NASA Langley for compression after impact loading [4] was implemented. The impactor consisted of three basic parts: a 51 mm (2 in.) diameter steel rod, an instrumented section, and a 12.7 mm (1/2 in.) diameter steel spherical tip. The instrumented section , or tup, was capable of measuring the impact force. This impact force was recorded using a digital data storage scope. The data was then reduced on a desk top PC using commercial software.
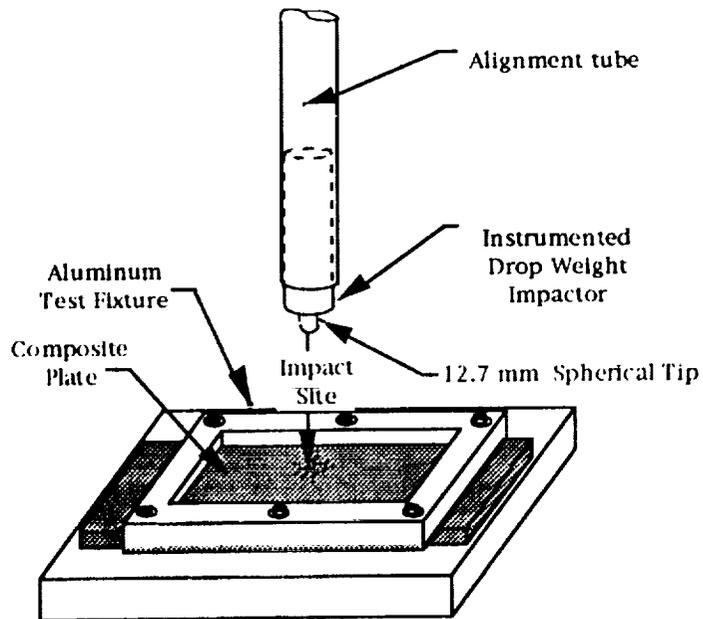

Figure 6. Typical Instrumented Impactor Setup.

The 10.16 x 15.24 cm (4 x 6 in.) panels were clamped in an aluminum picture frame for impacting. The clamping bolts were torqued tight to 2.87 J (80 in•lbs). This fixture is illustrated in Figure 6. The instrumented impactor was centered above the panel at the required height to impart the desired impact energy. After the impactor struck the specimen, a dummy panel was quickly moved between the fixture and specimen to prevent the impactor from repeatedly hitting the panel.

All specimens were ultrasonically C-scanned before impact to ensure that the panels were of high quality, free from manufacturing defects that would lead to premature failure. C-scans after impact as well as radiographs were used to determine the extent of the impact damage. Dent depths and damage areas from C-scans as well as peak impact forces and back face strains are given in Table 1 for each of the impact events. Impact energies of 13.56, 40.67, and 54.23 J (10, 30, & 40 ft•lbs) were used on the compression specimens. These impact energies were chosen to yield a variety of damage sizes and dent depths in the specimens. Dent depths were measured with a dial indicator mounted perpendicular to the surface of the plate. The tip of the gage was slid over the plate surface, through the impacted region. The maximum deflection, to the nearest one thousandth of an inch, was recorded.

Discussion of Results

Impacting of Compression Specimens

A comparison of both dent depth and average damage diameter is made against gross compressive stress in Figure 7. This data is also presented in tabular form in Table 3. The values plotted at zero on the ordinate axis are the results from unnotched test specimens. Curves were fit to the data and each data point

represents a single test specimen. Damage diameter, for this comparison, was calculated assuming the impact damage site to be round. In actuality the damage was always elliptical in shape but for this comparison, an assumption of roundness will allow us to make a linear comparison, rather than using a quadratic form.

Figure 7 shows that initially, gross compressive stress decreases sharply with increasing dent depth. After a dent depth of about 1.5 mm (0.06 in.), the loss in compressive strength is minimal. The Air Force specifies that no impairment in strength should result from a 2.5 mm. (0.1 in.) dent depth in a composite structure made from prepreg tape [5]. Thus, a 2.5 mm. (0.1 in.) deep dent might be considered "visible damage". An area bounding this region is shown in Figure 7. The vertical line would represents a design limit compressive stress based on this visible damage criteria.
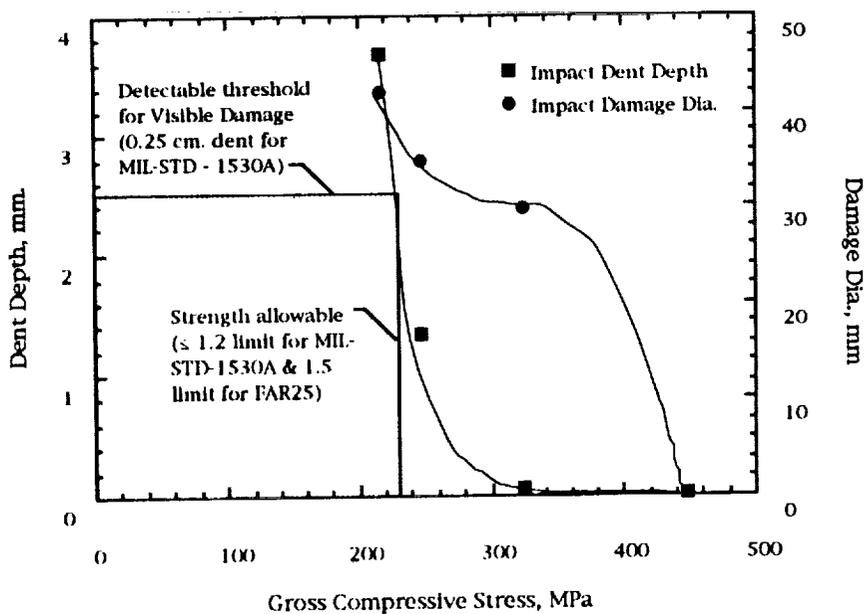

Figure 7. A Comparison of Impact Dent Depth and Damage Diameter to Compressive Failure Stress.

On the other hand, compressive stress initially decreases gradually with increasing damage diameter but drops sharply at

about 2.5 mm. (0.1 in.) which coincides with visible dent formation.

Impact energies of 13.56, 40.67, and 54.23 J (10, 30, & 40 ft•lbs) were used on the compression specimens to yield a variety of damage sizes and dent depths The smallest impact energy, 13.56 J, was low enough to yield no visible surface damage on either face while still producing an average damage area from C-scan of 596 mm.^{2} (0.92 in.^{2}) (see table 3). Dent depths for the 13.56 J impacts averaged only 0.0766 mm. (0.003 in.). This shallow dent was virtually indiscernible to the naked eye.

The 40.67 J impact energy produced an average damage area of 901 mm.^{2} (1.4 in.^{2}). This is a 51% increase in damage area from a 9% increase in average peak impact force. Average peak impact forces as well as back face strain are given in Table 3 for each of the impact events. The dent depth resulting from impact averaged 1.28 mm. (0.05 in.) for the 40.67 J impacts. This is 16 times the average depth of the 13.56 J impacts but is still less than the Air Force specification for tape materials.

The upper energy of 54.23 J was required to produce a dent deeper than 0.25 cm (0.1 inch). The average for this energy level was .274 cm. (0.11 in.). This impact energy was sufficient to produce sever back face damage, resulting in gross fiber breakage and local matrix damage at the impact site. The average damage area from C-scan was 1420 mm.^{2} (2.2 in.^{2}).

Unnotched Fatigue: Tension Specimens

The response of the unimpacted material to tension-tension fatigue is illustrated in Figure 8. Results are also listed in Table 2. The values plotted at one cycle are the static failure stresses from six monotonic room temperature tension tests reported in Table 2. A polynomial curve was fit to the data. Each of the data points

represents a single test specimen. The 3-D braids experienced a reduction in tensile strength with constant amplitude tension fatigue cycles of between 21 and 22% at 10^6 cycles. Static tension strength is about 1.5 times that of the static compression strength. The tensile strength reduction as a result of cyclic loading was also less than of the compression fatigue data. The fatigue response of this material suggests that although the off-axis yarns may delaminate or fail early in the life, the strength, being mostly dependent upon the 0° fibers, retains most of its initial value.
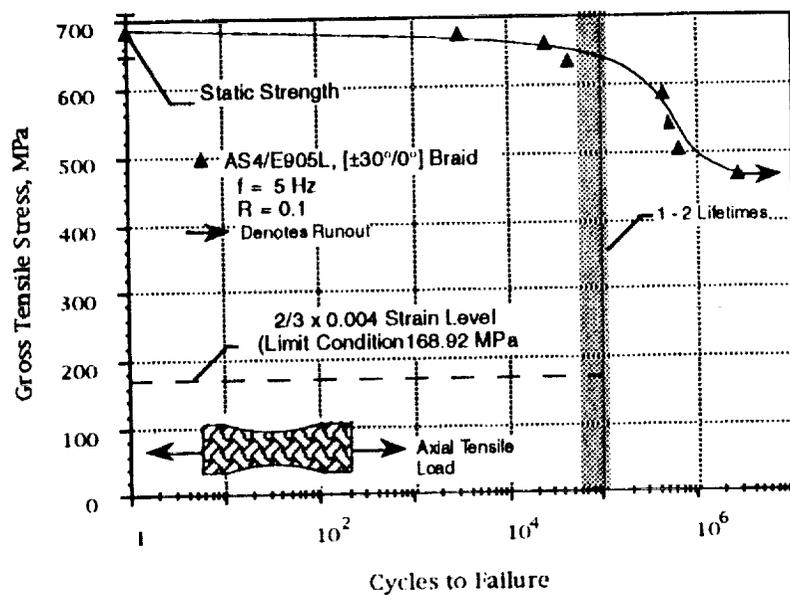
Figure 8. UnnotchedTension Fatigue of 3D Braids

Airframe manufactures typically design aircraft for a fatigue life that corresponds to two design economic lifetimes. One lifetime may be approximately 20 years or 60,000 flights, dependent on the aircraft design usage [5]. For this comparison one flight is assumed to equal to one constant amplitude fatigue cycle. A design allowable of 0.004 strain has been suggested for tape laminates on the basis of damage tolerance. To evaluate the fatigue performance of this braided material, a region covering one to two lifetimes has been shaded and a dashed line placed at a $\frac{2}{3}$ x 0.004 strain level (limit condition), based on the materials

14

initial modulus. At one lifetime, the fatigue strength is about 3.8 times the limit stress. For wing bending on a typical transport aircraft, the strains reach limit condition only a few times in a lifetime, which is much less than 60,000 cycles. Therefore, a design using this [±30°/0°] braid as an integral part of a composite wing, such as a spar or a frame, would have more than adequate fatigue strength.

Unnotched Fatigue : Compression Testing

The response of the undamaged material to compression-compression fatigue loading is displayed in Figure 9. The fatigue test results are listed in Table 2. Each of the data points represent a single test specimen. The values plotted at one cycle are averages of the static failure stresses from eight room temperature monotonic compression tests [6]. These averages are reported in Table 2. Logarithmic curve fits to the data are also plotted. At 10^6 cycles, the fatigue strengths were 43% to 44% less than the static values.
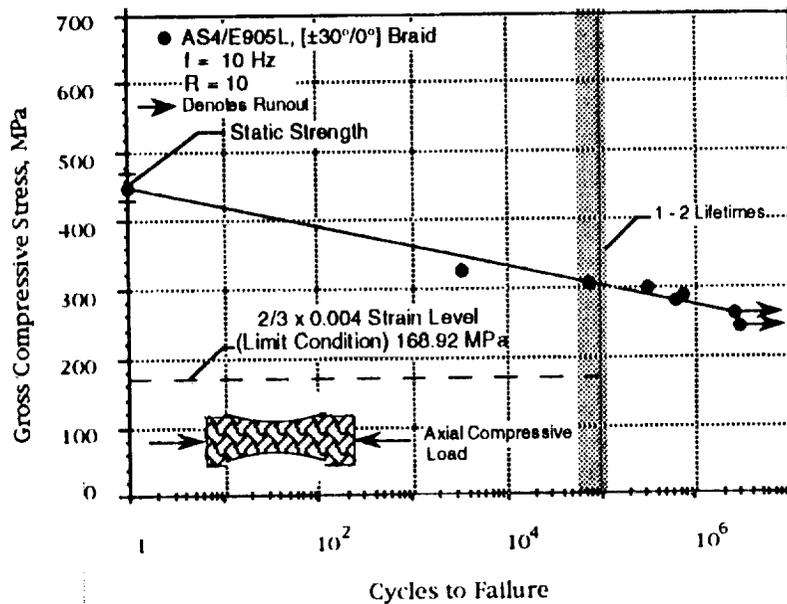
Figure 9. Unnotched Compression Fatigue of 3D Braids

15

Again, a region representing one to two design lifetimes has been shaded and the design limit strain of $\frac{2}{3}$ x 0.004 is shown. At one lifetime, the fatigue strength is about 1.8 times the limit stress. The unnotched compression fatigue response of this [±30°/0°] braid is barely adequate.

Post-Impact Fatigue: Compression Specimens

The compression-compression fatigue response of the impacted coupons is displayed in Figure 10. The values plotted at one cycle are the static failure stresses from the room temperature compression after impact tests which are also reported in Table 3. Data for impact energies of 13.56, 40.67, and 54.23 J (10, 30, & 40 ft•lbs) are shown. Each data point represents a single test specimen. Logarithmic curve fits to the data are also plotted.

Figure 10. Post-Impact Compression Fatigue of 3D Braids

Examination of the 40.67 J impact data in Figure 10 shows that at 10^6 cycles, the strengths were 33 to 34% less than the static values. This response is better than that obtained from the unnotched specimens or that obtained with a conventional tape laminate [7]. The 13.56 J and 54.23 J data curves show an even greater retention of their original static strength. At 10^6 cycles, the 13.56 J data and the 54.23 J data had lost only 21 to 23% of their static strength following the impact.
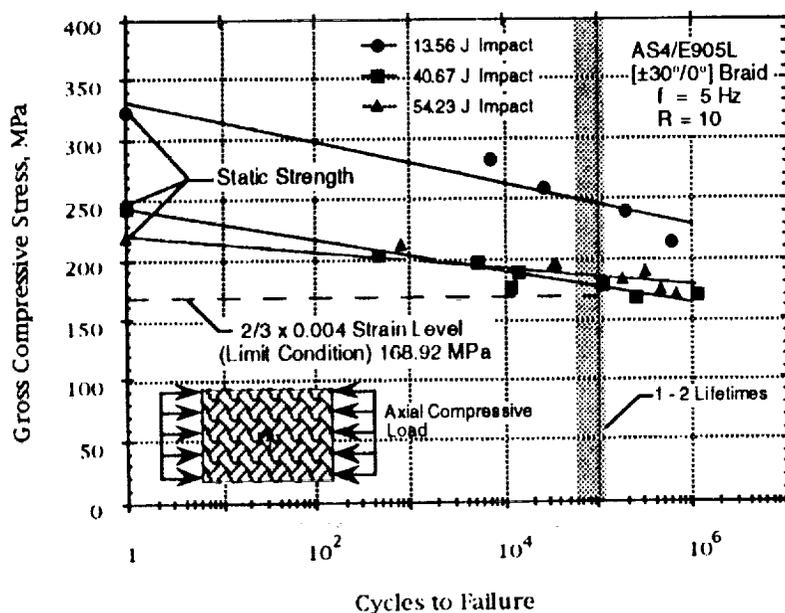
Again, a region representing one to two design lifetimes has been shaded and the design limit strain of $\frac{2}{3}$ x 0.004 is shown. The post-impact compression static strengths for impact energies of 13.56, 40.67, and 54.23 J (10, 30, & 40 ft•lbs) are approximately 28, 45, and 53% below the unnotched strength of this 3-D braid, respectively. The post-impact compression fatigue response of this material is marginally adequate at the higher impact energies. The 40.67 and 54.23 J data produce fatigue lives that are right at the thresholds displayed on Figure 10. Only the 13.56 J data is well within the acceptable region. The 54.23 J impacts however, tend to be classified in the realm of "visible damage" and thus would be repaired and so the fatigue lives would be irrelevant.

Damage Initiation and Progression

Stiffness loss will be discussed for three different cyclic ranges; low cycle, mid-range, and high cycle or specimen run-out. Low cycle fatigue, for purposes of this program, is defined as a cyclic life of less than ten thousand cycles. Mid range is defined as a cyclic life between 10 thousand and 500 thousand cycles. High cycle is defined as a cyclic life between 500 thousand and 10^6 cycles.

17

Unnotched Tension Fatigue

Figure 11 is a plot of typical high cycle and low cycle fatigue test results. Stiffness loss for a runout specimen was not measured. The tension fatigue specimens exhibited faster initial stiffness loss rates then the compression specimens. The loss of stiffness was immediate.

For low cycle fatigue, the average loss of elastic modulus ranged from 3% to 5% within the first 20% of the fatigue life. Edge damage was observed almost immediately and seemed to propagate at a fairly constant rate. The stiffness loss curve in Figure 11 does tend to flatten out at the first third of the fatigue life but declines afterwards at a faster rate. This response was typical of all the low cycle unnotched tension test specimens. Visually, damage was not apparent on the specimen's surface but was concentrated at the edge of the specimen.
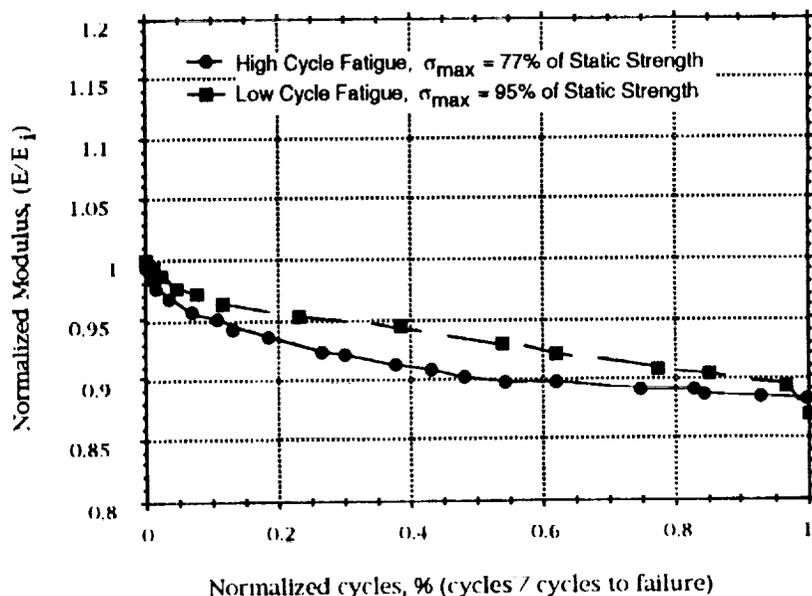

Normalized cycles, % (cycles / cycles to failure)

Figure 11. Normalized Unnotched Tension Modulus -vs- Normalized Life for High Cycle and Low Cycle Fatigue.

18

For the high cycle fatigue, edge damage was observed early but grew little thereafter. Examination of Figure 11 reveals that the stiffness drops 6% to 8% during the first 20% of the fatigue life. There was little damage growth along the surface of the coupon until late in the fatigue life. Some edge damage was observed mid-way in the life but did not appear to grow across the width or through the thickness to any significant degree until late in the life of the coupon.

Regardless of cyclic life, near final failure, damage consisted of matrix cracks between tows on the surface of the specimen adjacent to the edge damage. At failure, specimens for both high and low cycle tests retained 86% to 89% of their initial elastic modulus. Postmortem inspection of the specimens revealed fiber pullout and fractured fibers, along with severe matrix damage. The matrix cracks had run from the specimens free edge towards the center of the specimen, following the ±30° braid angle.

Unnotched Compression Fatigue

Because of the small distance between the hydraulic grips, it was not possible to make radiographs of the unnotched specimens without removing the specimens from the testing machine. Thus, damage was monitored visually and through stiffness loss curves.

Compliance change during cyclic loading provides a measure of damage accumulation. Figure 12 is a plot of normalized modulus versus the normalized cycle count for a typical high cycle, low cycle and run-out compression-compression fatigue test.
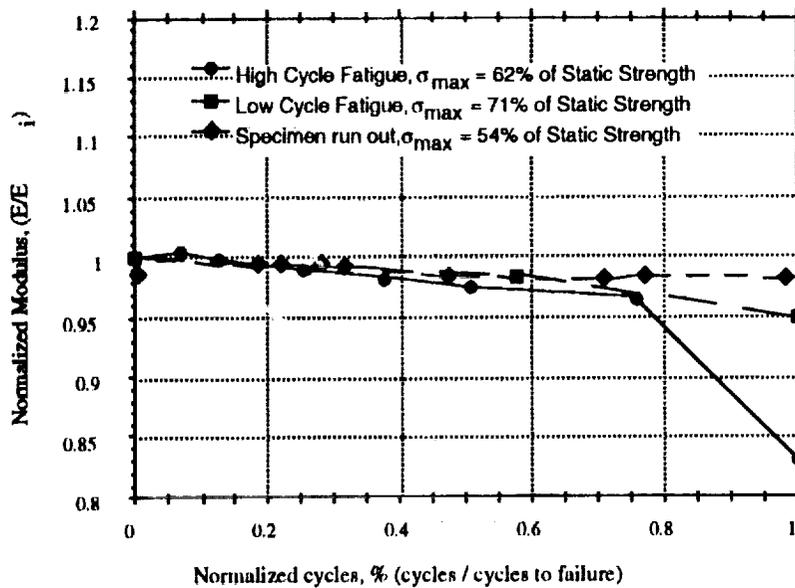
Figure 12. Normalized Unnotched Compression Modulus -vs-
Normalized Life for High Cycle, Low Cycle, Run-out
Fatigue.

Regardless of cyclic range, stiffness loss started early and it progressed very slowly. The material typically retained 96% of its original elastic modulus for 75% of its fatigue life. There were differences however between the ranges. Examination of Figure 12 shows that the stiffness drops rapidly after about 75% of life with high cycle fatigue. Surface damage also developed very rapidly at this point. At failure, the loss of elastic modulus ranged from 16 to 18.5%. Surface damage was not observed during low cycle fatigue and the loss of elastic modulus ranged from 4.5 to 6% at failure. For specimen runout (> 10^6 cycles) modulus declined by 1 to 3%. Some edge surface damage was observed mid-way in the life but did not appear to grow across the width or through the thickness to any significant degree.

20

Post-Impact Compression Fatigue

Damage was monitored visually, through radiographs, and through stiffness loss curves. The specimen stiffness was monitored in situ throughout the fatigue life, including the fracture cycle. Radiographs were taken simultaneously with the modulus measurements.

Figure 13 is a plot of normalized modulus versus normalized life for low cycle, mid-range, and high cycle. For low cycle specimens, modulus changed little through-out approximately 98% of life. During the last 2 or 3% of life, modulus typically declined 5 to 7%. Mid-range and high cycle specimens displayed similar stiffness loss characteristics. These specimens typically lost 12 to 18% of their original stiffness at failure. They differed from low cycle fatigue specimens by a loss of stiffness at an early percentage of their lives. The elastic modulus started to decrease right away, decreasing almost linearly throughout 85% of life. At failure, stiffness had declined dramatically.

Figure 14 is a montage of radiographs of the impact zone during various stages of fatigue life. The percentage of life is cycle count divided by cycles to failure. The percentage of size increase was determined by the method previously described (see Figure 5). Inspection of this figure reveals the increase in damage area as a function of cyclic stress. The example used is typical for a mid-range cyclic stress state. Note that the damage growth is always greatest late in the fatigue life.

Normalized cycles, % (cycles / cycles to failure)
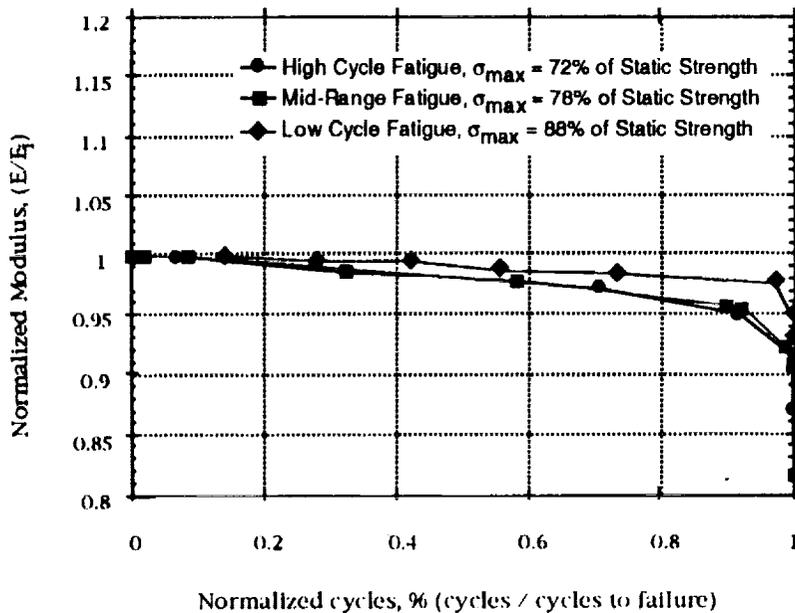
Figure 13. Normalized Post-Impact Compression Modulus
-vs- Normalized Life for High Cycle, Mid Cycle,
and Low Cycle Fatigue.

22

0% Of Life	21% Of Life	47% Of Life
0% Size Increase	7.4% Size Increase	13% Size Increase
68% Of Life	75% Of Life	90% Of Life
24% Size Increase	44% Size Increase	53% Size Increase
94% Of Life	99% Of Life	One Cycle Before Failure
59% Size Increase	79% Size Increase	91% Size Increase
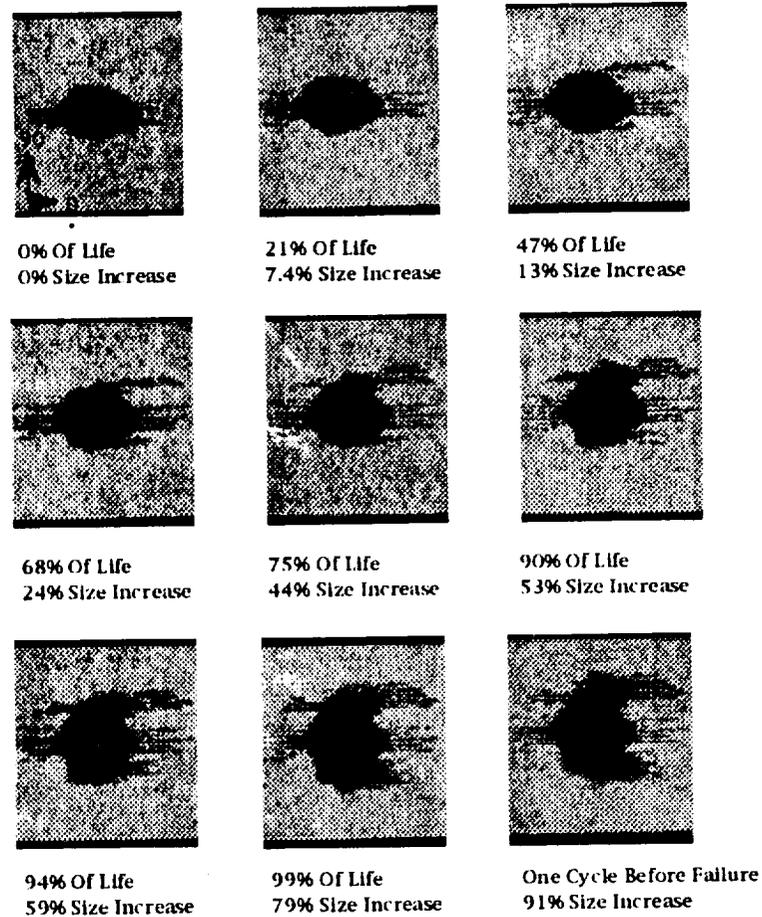
Figure 14. Dye Enhanced Radiographs of Damage Progression During Fatigue Cycling of Compression After Impact Specimens

Figure 15 is a plot of damage area growth revealed by dye enhanced radiography versus normalized life for the same three specimens used in Figure 13. The initial (static) damage area calculated from the impacts (Table 2) is not much different than that obtained from tape laminates [7] of similar constituents impacted at equivalent energy levels.

23

For the high cycle fatigue specimens, approximately 50% of the damage growth was seen in the last 10% of the fatigue life. Examination of radiographs along with visual observations show that damage growth in the high cycle fatigue specimens was almost nonexistent up to 85% of the fatigue life. At this point, growth was noticed moving mostly outward from the impact site, following the ±30° braids, towards the specimens edge.

Damage growth in the mid-range specimens, as displayed in Figure 13, shows that progression typically started much earlier, percentage wise, than with the high cycle specimens, but then subsided until 60 to 80% of the fatigue life. At this point the growth rate increased dramatically, typically to a point three times it's original size. In contrast, visual observations of the specimens surface showed damage growth to be slow but consistent.

Normalized cycles, %, (cycles / cycles to failure)

Figure 15. Normalized Post-Impact Damage Area -vs- Normalized Life for High Cycle, Mid Cycle, and Low Cycle Fatigue.

24

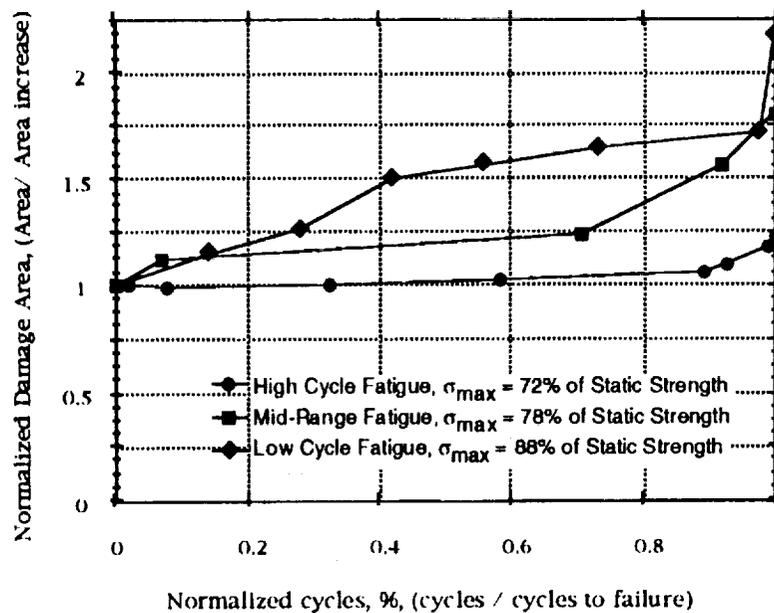With low cycle fatigue, damage growth began immediately and increased through approximately 95% of it's life. At this point, damage growth became unstable. Examination of the radiographs along with visual observations revealed that damage in the low cycle fatigue specimens grew mostly above and slightly outward from the impact site. This resulted in an increasing damage area while the majority of the load carrying area of the specimen remained unchanged.

Note that in all stress states, damage grew mostly on the convex side of the specimen (side opposite impact site), regardless of which way the specimen was mounted in the load frame. Damage grew one braid at a time, across the width, following the ±30° braid angle. Matrix cracks, created during impacting, grew first along the resin rich paths next to the zero degree tows (see figure 14), above and below the damage zone.

Summary

An investigation was conducted to evaluate the fatigue performance of a 3-D braided composite with and without impact damage. Damage initiation and growth was documented through the application of radiography and ultrasonic through transmission (C-scan). The mechanisms leading to damage initiation were established and failure modes were determined. Stiffness and strength degradation were measured as a function of applied cycles. These results were compared to current demage tolerance design criteria for primary structures to determine if the degradation was beyond an acceptable level.

In general, the unnotched fatigue strength of this [±30°/0°] 3-D braided composite is adequate. The tension fatigue strengths were found to be 53% higher than the compression fatigue strengths. There was also a larger loss in tension than compression modulus with fatigue cycles.

25

With the unnotched specimens, loaded in either tension or compression fatigue, damage consisted of resin cracks within tows and resin rich areas. In laminated composites, under monotonic compressive loading the epoxy tends to crack and delaminate prior to overall failure [8]. In this material, matrix failure from fatigue loading was similar to that observed under static loading. Damage appeared to be very localized near the specimens edges on the front and back surfaces of the specimen. Surface damage was not observed during low cycle fatigue. Some edge surface damage was observed mid-way in the life but did not appear to grow across the width or through the thickness to any significant degree. Matrix cracks formed in the resin rich areas along the braided tows, running the length of the tow at the surface of the specimen. These tows appeared to lose their ability to support load at this point because they buckled on each consecutive loading cycle. No damage was seen to grow through the thickness of the specimen at its edge. Postmortem inspection of the fracture surface showed that the fracture typically ran along the ±30° braid angle towards the specimens edge, sometimes passing under those tows crossing the fracture path and sometimes turning parallel to them. Final failure of the specimen was by shear kinking of the undamaged tows.

From the impact itself, damage consisted of matrix cracks and broken fibers within tows. During cyclic loading, matrix failure was observed along tow bundles running along the ±30° braids from the impact site. Damage growth tended to follow the braids, skipping down a tow every so often as it migrated towards the outside edges of the plate. Only for the 13.56J (10 ft•lbs) impacts was damage growth observed in the loading direction. This growth was slight and only evident early in the fatigue life. Again postmortem inspection of the fracture surface showed that the fracture typically ran towards the specimen's edge, along the ±30° braid angle, sometimes passing under those tows crossing the fracture path and sometimes turning parallel to them. Final

failure of the specimen was by shear kinking of the undamaged tows.

Although the static compression strength of this 3-D braid was reduced as much as 53% as a result of a severe impact (54.23 J), the residual fatigue life was found to be sufficient to satisfy current composite damage tolerance design critera. At an impact energy of 54.23 J, the materials response exceeds a limit strain condition of 0.004 for two lifetimes.

References

1. Lubowinski, S.J. , and Poe, C.C. Jr.; "Fatigue Characterization of Stitched Graphite/Epoxy Composites", Fiber-Tex 1987 Conference Proceedings, November 3-6, 1987, pp. 253 - 271.

2. Dow, Marvin B. , Smith, Donald L.; "Properties of Two Composite Materials Made of Toughened Epoxy Resin and High Strain Fiber", NASA Technical Paper 2826, July 1988.

3. Portanova, Marc A.: "Tension and Compression Fatigue Response of Unnotched 3D Braided Composites", NASA Contractor Report 189678, August 1992.

4. "NASA/Aircraft Industry Standard Specification for Graphite Fiber/Toughened Thermoset Resin Composite Material", NASA Reference Publication 1142, June 1985 .

5. Lincon, J.:" Certification of Composites for Aircraft". NASA CP 10075, March 1991, pp 401-420.

6. Jerry W. Deaton; Susan M. Kullerd; M.A. Portanova; "Mechanical Characterization of 2-D, 2-D Stitched, and 3-D Braided / RTM Materials", Third NASA Advanced Composites Technology Conference, Long Beach, California, NASA CP 3178, June 8-11, 1992.

7. C.C. Poe, Jr.; M.A. Portanova; John E. Masters; W.C. Jackson; "Comparison of Impact Results for Several Polymeric Composites Over a Wide Range of Low Impact Velocities", First NASA Advanced Composites Technology Conference, NASA CP 3104, October 29 - November 1, 1990.

8. Guynn, E.G., and Bradley, W.L., "Measurements of the Stress Supported by the Crush Zone in Open Hole Composite Laminates Loaded in Compression," Journal of Reinforced and Plastics and Composites, volume 8, number 2, March 1989, pp.133-149.

28

Specimen # @ 13.56 J Impact Energy	C-Scan Damage Area, mm^2	Impact Dent Depth, mm.	Peak Impact Force, N	Back Face Strain, %
16L - CAI-15	697	0.063	9533	1.18
16L - CAI-16	542	0.081	8924	1.18
16L - CAI-17	581	0.089	9692	1.18
17U - CAI-18	574	0.069	10812	1.18
17U - CAI-19	619	0.061	9533	1.18
8U - CAI-20	561	0.097	9278	1.18
Average	596	0.077	9699	1.18
Std. Dev.	56	.015	688	0.0

Specimen # @ 40.67 J Impact Energy	C-Scan Damage Area, mm^2	Impact Dent Depth, mm.	Peak Impact Force, N	Back Face Strain, %
8L - CAI-1	1032	1.55	10720	1.18
8L - CAI-2	871	1.85	10323	1.18
8L - CAI-3	948	1.27	10125	1.18
9L - CAI-4	1006	0.97	11064	1.18
9L - CAI-5	839	1.34	10376	1.18
9L - CAI-6	858	0.92	11018	1.18
9L - CAI-7	755	1.07	10337	1.18
Average	901	1.29	10566	1.18
Std. Dev.	99	0.34	369	0.00

Specimen # @ 54.23 J Impact Energy	C-Scan Damage Area, mm^2	Impact Dent Depth, mm.	Peak Impact Force, N	Back Face Strain, %
17U - CAI-8	1375	1.90	---	---
16U - CAI-9	1375	2.51	10766	1.19
8U - CAI-10	1562	2.59	10795	1.19
16U - CAI-11	1430	2.59	11936	1.19
16U - CAI-12	1393	2.31	12049	1.19
17L - CAI-13	1414	3.56	9880	1.19
17L - CAI-14	1394	3.68	11248	1.19
Average	1420	2.74	11112	1.19
Std. Dev.	65	0.65	814	0.00

Table 1.　　Tabulated Impact Data for 13.56, 40.67, and 54.23 J
Impact Energies.

Compression Specimen ID	% of P_{static}	Cycles to Failure	Maximum Cyclic Stress, MPa	Maximum Cyclic 0° Strain, %	Initial Modulus GPa	In-situ Poisson's Ratio
ST	100	1	447 ±20	1.04	---	0.76
8U-UNC3	71.8	3,440	321	0.50	64.53	---
8U-UNC2	67.3	79,400	301	0.49	60.95	---
8U-UNC4	65.9	328,800	294	0.46	63.85	---
8U-UNC1	63.3	779,000	283	0.43	65.98	0.71
8L-UNC5	61.3	612,000	274	0.36	67.91	0.73
8L-UNC7	57.3	*2.7 E6	256	0.32	74.53	---
8L-UNC6	53.7	*3.1 E6	240	0.29	68.67	0.69

Tension Specimen ID	% of P_{static}	Cycles to Failure	Maximum Cyclic Stress, MPa	Maximum Cyclic 0° Strain, %	Initial Modulus GPa	In-situ Poisson's Ratio
ST	100	1	681 ±32	1.075	63.98	0.99
15L-UNT2	96.9	3,210	658	0.949	77.70	---
15L-UNT7	94.8	25,900	646	0.932	78.26	0.82
15L-UNT6	91.2	46,800	621	0.945	73.57	0.80
15L-UNT5	84.2	468,000	574	0.950	89.22	0.80
15L-UNT4	77.9	548,700	531	0.690	77.50	---
15L-UNT3	72.0	670,000	491	0.627	75.08	---
15L-UNT1	66.9	*2.8 E6	456	0.487	84.12	---

Table 2.   Unnotched Compression & Tension Fatigue Test Results
* denotes runout.
ST denotes Static test.
UNT denotes unnotched tension.
UNC denotes unnotched compression.

Post-Impact Compression Fatigue Specimen ID	% of P_{static}	Cycles to Failure	Maximum Cyclic Stress, MPa	Maximum Cyclic 0° Strain, $\Delta \ell / \ell$, %	Initial Modulus GPa
8L-SIC-30	100	1	247	0.91	35.17
9L - CAI-5	85	480	207	1.02	34.99
9L - CAI-6	81.4	5001	198	0.887	36.05
9L - CAI-4	78	14200	189	0.857	34.30
8L - CAI-1	75	119000	182	1.080	36.36
8L - CAI-3	72.5	124000	176	0.928	36.12
8L - CAI-2	70	1130000	170	0.730	34.04
9L - CAI-7	69	244000	167	0.892	34.79
7U-SIC-14	100	1	216	0.873	24.75
17L - CAI-13	98	840	208	0.828	37.57
16U - CAI-12	90	36000	194	0.618	39.92
8U - CAI-10	87.5	334000	189	0.825	37.16
16U - CAI-9	84.4	189000	182	0.726	39.92
17U - CAI-8	81.7	471000	176	0.484	38.81
16U - CAI-11	77.6	650000	167	0.440	40.67
17L-SIC-10	---	---	---	---	28.33
16L - SIC-15	100	1	324	0.974	34.19
17U - CAI-19	88	7180	285	0.779	40.12
16L - CAI-17	80	27200	259	0.783	33.16
17U - CAI-18	75	201000	242	0.715	34.33
16L - CAI-16	66	664000	214	0.632	33.85

Table 3.   Post-Impact Compression Fatigue Test Results
* denotes runout.
SIC denotes Static test.
Specimen ID prefix denotes plate number.
CAI denotes compression after impact.

REPORT DOCUMENTATION PAGE		*Form Approved* *OMB No. 0704-0188*

1. AGENCY USE ONLY (*Leave blank*)	2. REPORT DATE January 1994	3. REPORT TYPE AND DATES COVERED Contractor Report	

4. TITLE AND SUBTITLE Fatigue Resistance of Unnotched and Post Impact [± 30°/0°] 3-D Braided Composites	5. FUNDING NUMBERS NAS1-19000 WU 510-02-12-09
6. AUTHOR(S) Marc A. Portanova	

7. PERFORMING ORGANIZATION NAME(S) AND ADDRESS(ES) Lockheed Engineering and Sciences Company Hampton, VA 23666	8. PERFORMING ORGANIZATION REPORT NUMBER

9. SPONSORING / MONITORING AGENCY NAME(S) AND ADDRESS(ES) National Aeronautics and Space Administration Langley Research Center Hampton, VA 23681-0001	10. SPONSORING / MONITORING AGENCY REPORT NUMBER NASA CR 191590

11. SUPPLEMENTARY NOTES

Langley Technical Monitor: Charles E. Harris
Final Report

12a. DISTRIBUTION / AVAILABILITY STATEMENT Unclassified - Unlimited Subject Category - 24	12b. DISTRIBUTION CODE

13. ABSTRACT (*Maximum 200 words*)

The fatigue resistance of a multiaxial braided (3-D) graphite/expoxy composite in both unnotched and post impacted conditions has been evaluated. The material tested is a [±30°/0°] multiaxial braid constructed from AS4/12K tow graphite fibers and British Petroleum E905L epoxy resin. These materials were braided as dry preforms and the epoxy was added using a resin transfer moulding process (RTM). The unnotched and post-impact specimens were tested in compression-compression fatigue at 10 Hz with a stress ration of R=10. The unnotched tension-tension fatigue specimens were tested at 5 Hz with a stress ration of R=0.1. Damage initiation and growth was documented through the application of radiography and ultrasonic through transmission (C-scans). Visible inspection of surface and edge damage was also noted to describe the initiation and progression of damage in these materials. The mechanisms leading to damage initiation were established and failure modes were determined. Stiffness and strength degradation were measured as a function of applied cycles. These 3-D braided composite results were compared to strain levels currently used to design primary structure in commercial aircraft composite components made from prepreg tape and autoclave cured.

14. SUBJECT TERMS Braided composites; Tension fatigue; Compression fatigue; Low velocity impact; Damage mechanisms			15. NUMBER OF PAGES 32
			16. PRICE CODE A03

17. SECURITY CLASSIFICATION OF REPORT Unclassified	18. SECURITY CLASSIFICATION OF THIS PAGE Unclassified	19. SECURITY CLASSIFICATION OF ABSTRACT	20. LIMITATION OF ABSTRACT